A Study of Predictable Patterns for Seasonal Forecasting of New Zealand Rainfall

XIAOGU ZHENG

National Institute of Water and Atmospheric Research, Wellington, New Zealand

CARSTEN S. FREDERIKSEN

Bureau of Meteorology Research Centre, Melbourne, Australia

(Manuscript received 19 April 2005, in final form 19 September 2005)

ABSTRACT

A recently developed variance decomposition approach is applied to study the causes of the predictability of New Zealand seasonal mean rainfall. In terms of predictability, the Southern Oscillation is identified as being the most important cause of variability for both the winter and summer New Zealand rainfall, especially for the North Island. Indian Ocean sea surface temperature variability and the Southern Hemisphere annular mode are the second most important causes of variability for winter and summer rainfall, respectively.

Based on this study, a statistical prediction scheme has been developed. May Niño-3 (5°N–5°S, 150°–90°W) SSTs and March–May (MAM) central Indian Ocean SSTs are identified as being the most important predictors for the winter rainfall, while September–November (SON) Niño-3 SSTs, November local New Zealand SSTs, and the SON Southern Hemisphere annular mode index are the most important predictors for the summer rainfall. The predictive skill, in term of the percentage explained variance for the verification period (1993–2000) is nearly 20%, which is considerably higher than that achieved previously.

1. Introduction

Because much of New Zealand (NZ) economic activity is dependent on agriculture, tourism, and other climate-sensitive industries, skillful seasonal forecasts of temperature and rainfall have obvious potential benefits for the country. While forecast schemes of NZ temperature are relatively successful, NZ rainfall has proven to be more difficult to forecast (Zheng and Renwick 2003). A number of authors have tried to find relationships between NZ rainfall variability and large-scale sea surface temperature (SST) forcing or persistence in the Southern Hemisphere circulation. For example, Gordon (1986) and Mullan (1995) have looked at relationships with El Niño–Southern Oscillation (ENSO), Mullan (1998) have looked at the role of Indian Ocean variability; and Kidson and Gordon (1986) and Francis and Renwick (1998) have considered persistence in the circulation.

Corresponding author address: Xiaogu Zheng, National Institute of Water and Atmospheric Research, Private Bag 14901 Kilbirnie, Wellington, New Zealand.
E-mail: x.zheng@niwa.co.nz

In the extratropics, it is known that a substantial component of interannual variability of seasonal mean fields arises from variability within the season (see, e.g., Madden 1981; Zheng et al. 2004). Day-to-day weather variability with a time scale longer than the deterministic prediction period (about 10 days) mainly contributes to this component, and therefore it is essentially unpredictable on seasonal, or longer, time scales. For this reason, this component is called the "intraseasonal component" (Zheng and Frederiksen 2004) or the "weather noise component" (Madden 1976; Zheng and Frederiksen 1999). After removing this component from seasonal mean fields, the residual component is more likely to be associated with slowly varying external forcings on the climate system (e.g., SST) and slowly varying (interannual/supra-annual, slower-than-intraseasonal time scale) internal atmospheric variability, and therefore it is more potentially predictable at long ranges (Madden 1976). For this reason, the residual component of the seasonal mean fields is called the "slow component" (Zheng and Frederiksen 2004), or the potentially predictable component (Madden 1976; Zheng and Frederiksen 1999).

Zheng and Frederiksen (2004) recently developed a

methodology for estimating spatial patterns of slow and intraseasonal components from monthly mean data. This methodology provides a way to better identify and understand the sources of predictive skill as well as the sources of uncertainty in climate variability. Here, we illustrate this by applying the methodology to an analysis of NZ rainfall variability and show how the information obtained can be used to improve seasonal forecasts. Because seasonal mean rainfall is closely related to local or hemispheric mean pressure fields, we have applied the technique to the cross-covariance matrix between NZ seasonal mean rainfall and hemispheric seasonal mean sea level pressure (MSLP). In this way, the dominant coupled patterns of the slow components capture the important relationships between the slow components of both the NZ rainfall and the hemispheric circulation, and also possible external forcings. As we show below, this type of analysis can help to better identify possible predictors of NZ rainfall and construct an improved statistical prediction scheme.

The paper is arranged as follows. Data and methodology are described in sections 2 and 3, respectively. The analysis results are documented in section 4, and the proposed prediction scheme is studied in section 5. Our conclusions are in section 6.

2. Datasets

In this section, we introduce the datasets employed in the coupled analysis, and also the SST dataset used to identify possible SST forcing, or SST predictors, of the rainfall variability.

a. New Zealand rainfall

The monthly New Zealand rainfall used in this study has been calculated from observed daily rainfall totals of about 100 rainfall stations taken from the New Zealand Climate Database operated by the National Institute of Water and Atmospheric Research. The monthly rainfall is expressed as a fraction of the 1961–90 average for a particular month. As in earlier studies of New Zealand regional climate variability (e.g., Salinger 1980; Mullan 1998; Zheng and Renwick 2003), we shall consider New Zealand as consisting of six regions (see, e.g., Zheng and Renwick 2003, their Fig. 1) where the regional definitions follow natural topographic boundaries. They correspond roughly to the north, west, and east of both islands. Thus, our monthly rainfall dataset consists of rainfall averages over these six regions. The total period used is the 48 years of March 1953–February 2001.

The methodology, described in Zheng et al. (2004) and Zheng and Frederiksen (2004), uses a moment estimation approach to estimate the covariability between two intraseasonal component series. While this is a more general approach than maximum likelihood estimation (Zheng et al. 2000), in that it does not assume that the intraseasonal component is normally distributed, the estimation error may be large if the intraseasonal component has a distribution that is skewed or heavily tailed. This is the case for the raw daily New Zealand rainfall, and also for the monthly means. One way to overcome this is to rank the data into a number of categories, which produces a more uniform distribution. Here, the 48 yr of rainfall data for each region and each month has been divided into 24 consecutive categories with two data in each category.

b. Reanalysis data

The monthly mean MSLP dataset used in the coupled analysis is taken from the National Centers for Environmental Prediction–National Center for Atmospheric Research (NCEP–NCAR) reanalyses (Kalnay et al. 1996) over the period of March 1953 through February 2001, and has been subsampled on a 5° latitude × 5° longitude grid. As in Frederiksen and Zheng (2004), a variable resolution in longitude has been used in order to avoid biasing the analysis toward high latitudes. In the Southern Hemisphere, the longitude spacing is taken as 5° between 0° and 45°S, 10° between 50° and 65°S, 15° at 70°S, 20° at 75°S, 30° at 80°S, 60° at 85°S, and a single point at the pole. Monthly means of MSLP at each grid point and for each month have been standardized using the standard deviation over all 48 yr. Otherwise, the relationships derived may be dominated by regional pressure patterns with higher interannual variability but with less impact on NZ rainfall. We have also constructed a Southern Hemisphere annular mode index (SAMI; Thompson and Wallace 2000). This is defined as the zonal average of the standardized mean of the NCEP–NCAR MSLP difference between 45° and 65°S.

In addition, in order to aid in the physical interpretation of our coupled patterns, we have also used our methodology to relate them to the intraseasonal and slow components of the original global NCEP–NCAR reanalyses of the 500-hPa geopotential height field (on a 5° latitude × 5° longitude grid) for the same 48 yr period.

c. Sea surface temperature

The sea surface temperatures used in this study are taken from the Met Office Hadley Centre Sea Surface Temperature dataset (HADISST1.1; Rayner et al. 2003)

from March 1953 to February 2001 and have been subsampled on a 2° latitude × 2° longitude grid. The area used to produce the one-point correlation maps of section 4 is between 20°N and 60°S and between 20°E and 60°W.

3. Methodology

a. Decomposition of covariability

Zheng and Frederiksen (2004) proposed a methodology for extracting, from monthly mean data, spatial patterns of interannual (supra-annual) variability in seasonal mean fields that can be related to variability of slow and intraseasonal components. The interested reader is referred to this paper for a detailed description of the methodology. Here, we present only a brief summary of the method.

First, the annual cycle is removed from the data. The monthly time series of each climate anomaly is then conceptually decomposed into two components consisting of a seasonal "population" mean and a residual departure from this mean. Thus, if x_{ym} represents sample monthly values within a season, in month m ($m = 1, 2, 3$) in year y ($y = 1, \ldots, Y$, where Y is the total number of years), we use the following decomposition (Zheng et al. 2000; Zheng et al. 2004; Zheng and Frederiksen 2004):

$$x_{ym} = \mu_y + \varepsilon_{ym}. \tag{1}$$

Here, μ_y is the seasonal population mean in year y, and ε_{ym} is a residual monthly departure of x_{ym} from μ_y and arises from intraseasonal variability. The vector $\{\varepsilon_{y1}, \varepsilon_{y2}, \varepsilon_{y3}\}$ is assumed to comprise a stationary and independent annual random vector with respect to year. Equation (1) implies that month-to-month fluctuations, or intraseasonal variability, arise entirely from $\{\varepsilon_{y1}, \varepsilon_{y2}, \varepsilon_{y3}\}$ (e.g., $x_{y1} - x_{y2} = \varepsilon_{y1} - \varepsilon_{y2}$).

We represent an average taken over an independent variable (i.e., m or y) by replacing that variable subscript with "o." For example, x_{yo} indicates the seasonal average of x_{ym} in year y and x_{oo}, the average of x_{ym} taken over all months and years. With this notation, a seasonal mean can be expressed as

$$x_{yo} = \mu_y + \varepsilon_{yo}, \tag{2}$$

where ε_{yo} is associated with intraseasonal variability and μ_y with the interannual variability of external forcings and slowly varying (interannual/supra-annual) internal dynamics. Zheng and Frederiksen (2004) refer to these as the intraseasonal and "slow" components, respectively, of the seasonal mean x_{yo}, which is also referred to as the "total" component.

Suppose now that we have two climate variables x_{ym} and x'_{ym} that satisfy Eqs. (1) and (2). Then, Zheng and Frederiksen (2004) derived the following estimate of the interannual covariance $V(\varepsilon_{yo}, \varepsilon'_{yo})$ of the intraseasonal components,

$$V(\varepsilon_{yo}, \varepsilon'_{yo}) \approx \hat{\sigma}^2(3 + 4\hat{\phi})/9, \tag{3}$$

where

$$\hat{\sigma}^2 = \frac{a}{2(1 - \hat{\phi})}, \tag{4}$$

$$\hat{\phi} = \left[\frac{a + 2b}{2(a + b)}\right], \tag{5}$$

$$a = \frac{1}{2}\left[\frac{1}{Y}\sum_{y=1}^{Y}(x_{y1} - x_{y2})(x'_{y1} - x'_{y2}) + \frac{1}{Y}\sum_{y=1}^{Y}(x_{y2} - x_{y3})(x'_{y2} - x'_{y3})\right], \tag{6}$$

$$b = \frac{1}{2}\left[\frac{1}{Y}\sum_{y=1}^{Y}(x_{y1} - x_{y2})(x'_{y2} - x'_{y3}) + \frac{1}{Y}\sum_{y=1}^{Y}(x_{y2} - x_{y3})(x'_{y1} - x'_{y2})\right]. \tag{7}$$

To reduce the estimation error, the estimated $\hat{\phi}$ has to be constrained. If both x_{ym} and x'_{ym} are pressure variables, $\hat{\phi}$ is constrained to lie within the interval [0, 0.1] [see Zheng and Frederiksen (2004) for a detailed proof]. Otherwise (i.e., at least one of either x_{ym} or x'_{ym} is a rainfall variable), $\hat{\phi}$ is empirically constrained to lie within the interval [−0.1, 0.1].

Because the covariance between two seasonal means can be estimated as

$$V(x_{yo}, x'_{yo}) \approx \frac{1}{Y - 1}\sum_{y=1}^{Y}(x_{yo} - x_{oo})(x'_{yo} - x'_{oo}), \tag{8}$$

the covariance between two seasonal means can be decomposed, using Eq. (3), as

$$V(x_{yo}, x'_{yo}) = [V(x_{yo}, x'_{yo}) - V(\varepsilon_{yo}, \varepsilon'_{yo})] + V(\varepsilon_{yo}, \varepsilon'_{yo}), \tag{9}$$

where the first term on the right-hand side can be rewritten as

$$V(x_{yo}, x'_{yo}) - V(\varepsilon_{yo}, \varepsilon'_{yo}) = V(\mu_y, \mu'_y) + V(\mu_y, \varepsilon'_{yo}) + V(\mu'_y, \varepsilon_{yo}), \tag{10}$$

and will be referred to as the "residual" covariance after removing the variability of the intraseasonal com-

ponent. It is worth emphasizing that this covariance, in general, consists of not only the covariance between μ_y and μ'_y (i.e., the slow components of the climate variables), but also their interaction terms with ε_{yo} and ε'_{yo}. In the case where the intraseasonal and slow components are independent, the residual covariance reduces to the covariance of the slow component. When this is not the case, $V(x_{yo}, x'_{yo}) - V(\varepsilon_{yo}, \varepsilon'_{yo})$ may still be better related to the covariance between the two slow components than is $V(x_{yo}, x'_{yo})$.

Once the intraseasonal and residual cross-covariance matrices have been estimated, a singular value decomposition (SVD) analysis is conducted to derive the coupled patterns of variability. We shall refer to the pattern for each climate variable as the empirical orthogonal function (EOF) of that variable. The principal component (PC) time series of each climate variable can then be defined as the projection of the climate field, in each year and month, onto the EOF corresponding to that climate variable. The interested reader is referred to Zheng and Frederiksen (2004) for a more detailed description of the technicalities involved with the solution process.

In this study, we have found that although the components of rainfall variability are best related to the MSLP, the coupled MSLP patterns tend to be a little noisy. Hence, it is instructive to apply Eq. (3) and Eq. (10), respectively, to calculate the one-point covariance maps between the intraseasonal and slow components of the 500-hPa geopotential height field and the corresponding MSLP PC as a means of aiding the physical interpretation of our coupled patterns.

b. Rainfall prediction

Let column vector $\mathbf{r}_{ym}$ denote the rainfall field in month m and in year y and $\mathbf{V}$ denote the EOF matrix for rainfall derived from SVD analysis on the residual cross-covariance matrix [Eq. (9)] between MSLP and rainfall. Let $\mathbf{p}_y$ denote the projection of the rainfall field onto $\mathbf{V}$ in year y, that is,

$$\mathbf{p}_y \equiv \mathbf{r}_{yo}^{\mathrm{T}}\mathbf{V}. \tag{11}$$

Then, the rainfall field can be written as

$$\mathbf{r}_{yo}^{\mathrm{T}} = \mathbf{p}_y\mathbf{V}^T. \tag{12}$$

Matrix $\mathbf{V}$ can be estimated using MSLP and rainfall data in a training period. Therefore, the seasonal mean rainfall field $\mathbf{r}_{yo}$ can be predicted given a prediction of $\mathbf{p}_y$.

The skill s, relative to a baseline forecast (usually climatology), is defined as a ratio of sums of squares over a verification period:

$$s = \sum_i \sum_y [b_y(i) - o_y(i)]^2 \Big/ \sum_i \sum_y [p_y(i) - o_y(i)]^2, \tag{13}$$

where $o_y(i)$ is the observed value of the seasonal mean rainfall in year y and region i and $p_y(i)$ and $b_y(i)$ are the values predicted using a scheme and baseline climatology forecast, respectively. The percentage explained variance is then defined as

$$V_{\mathrm{expl}} = 100\left(1 - \frac{1}{s}\right), \tag{14}$$

(see Wilks 1995; Francis and Renwick 1998 for more details). In this study, the percentage explained variance will be used to evaluate the proposed prediction schemes.

4. Results

In this section, the methodology documented in section 3 is applied to derive the slow and intraseasonal patterns of New Zealand rainfall and the circulations associated with these rainfall patterns for June–August (JJA) and December–February (DJF), respectively. The ultimate aim of this analysis is to try to construct a better statistical prediction scheme for New Zealand rainfall based on the information obtained from the structure of these coupled patterns. To this end, we have also considered possible SST sources of predictability by constructing one-point correlation maps between the slow rainfall PCs (defined as the projections of the seasonal rainfall onto the slow rainfall patterns) and one-season-lead seasonal mean SST fields. The data period for the study in this section is from March 1953 to February 1992, which corresponds to the training period for our forecast scheme (see section 5).

a. JJA slow patterns

The covariability between New Zealand JJA rainfall and MSLP is dominated by the first two slowly coupled components, which explain 45% and 17%, respectively, of the covariability in the slow component. These two components also provide the majority of the skill of our predictive scheme (see section 5). Including other slow components adds negligible additional skill, and therefore we will not discuss these further here.

The first slow JJA rainfall pattern and the associated circulation (500-hPa height) are shown in Fig. 1a. At the phase shown here, the circulation pattern has posi-

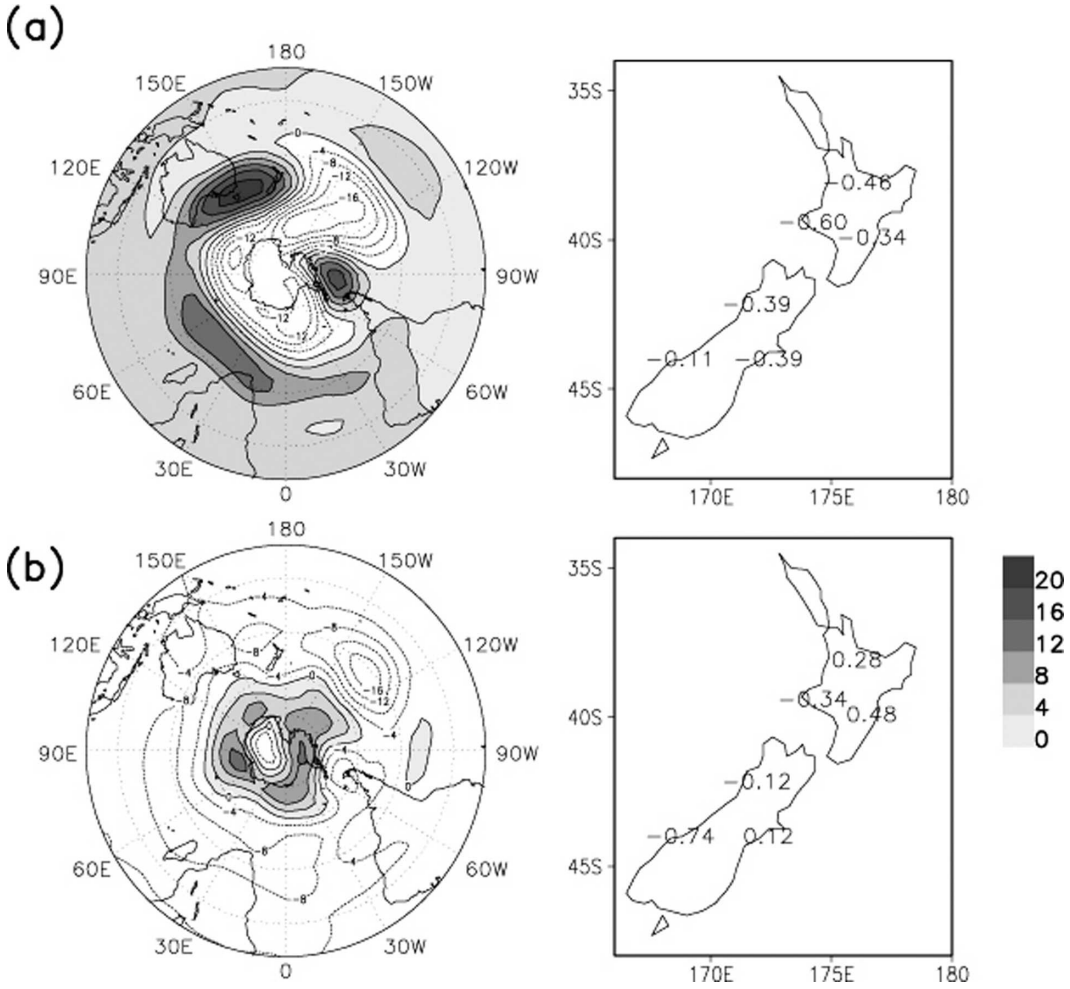

FIG. 1. Coupled JJA patterns of (a) EOF1 and (b) EOF2 for the slow modes of 500-hPa height and NZ rainfall. For the height field, positive contours are solid and shaded and negative contours are a dash line with labels. Contour interval is 4 m.

tive anomalies over NZ. In response, NZ is drier everywhere, especially in the north. This circulation pattern is clearly associated with El Niño variability with lower-than-normal pressure along 40°S throughout the Pacific and positive pressure anomalies south of Australia and Africa and in the area of the Bellingshausen Sea. This is very similar to the 500-hPa height pattern seen in Fig. 8.4(a) of Kiladis and Mo (1998) for a composite of 10 warm ENSO events. Karoly (1989) found a similar pattern in a composite of three ENSO events [his Fig. 2b]. Figure 2a shows the one-point correlation map between the slow rainfall PC1 and the March–May (MAM) SST. It indicates that this slow rainfall pattern is associated with a significant warming in the eastern tropical Pacific and central Indian Ocean during the previous season. There are also cooler SSTs surrounding New Zealand. At the opposite phase (La Niña) to that shown in Figs. 1a and 2a, wetter conditions than normal would prevail over New Zealand.

The second slow JJA rainfall pattern and the associated circulation are shown in Fig. 1b. The 500-hPa height pattern has an anomalous trough northwest of New Zealand, inducing enhanced northeasterly winds that result in wetter-than-normal conditions over the northeast of New Zealand. The higher-than-normal pressure at high latitudes south of New Zealand, together with the contrasting low and high pressure anomalies in the central Pacific, induces anomalous easterlies and consequently drier conditions west of the Alps and especially in the southwest. These conditions are reversed at the opposite phase to that shown in Fig. 1b. There is some suggestion in the 500-hPa height pattern of a wavenumber-3 pattern associated with the Southern Hemisphere annular mode [SAM; see, e.g.,

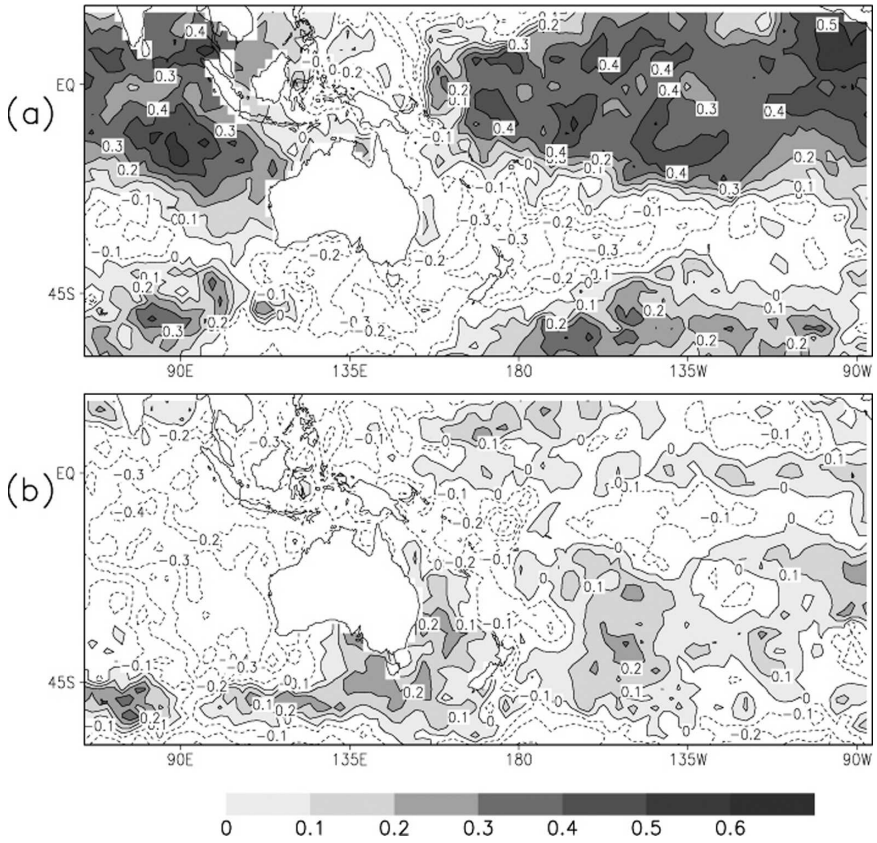

FIG. 2. One-point correlation maps of MAM SST with slow rainfall time series of (a) PC1 and (b) PC2 associated with slow modes EOF1 and EOF2, respectively. Contour interval is 0.1 and positive contours are shaded.

Fig. 8.3(a) of Kiladis and Mo 1998]. The one-point correlation map, between the slow rainfall PC2 and the MAM SST (Fig. 2b), shows that the central tropical and eastern subtropical Indian Ocean is significantly cooler at this phase, indicating a strong teleconnection between NZ rainfall and Indian Ocean SST variability.

b. DJF slow patterns

As for JJA, the first two dominant coupled patterns of New Zealand rainfall and MSLP provide most of the skill in our predictive scheme (see section 5), and therefore we will concentrate only on these two modes of covariability. They explain 39% and 20%, respectively, of the covariability in the slow component.

The first slow DJF rainfall pattern and the associated circulation are shown in Fig. 3a. Locally, the 500-hPa height pattern has an anomalous trough north of New Zealand and a ridge centered southwest of New Zealand, inducing enhanced northeasterly winds that result in wetter-than-normal conditions over the north of New Zealand, and drier conditions in the southwest. In the Tropics/subtropics, the 500-hPa height is generally lower over the entire hemisphere. At this phase, the height pattern is broadly similar to Fig. 8.5(c) of Kiladis and Mo (1998), which shows 500-hPa DJF height anomalies for a composite of six cold ENSO events. The first slow NZ rainfall pattern is also consistent with a cold event. This is further confirmed by the one-point correlation map between the slow rainfall PC1 and the September–November (SON) SST field (Fig. 4a). Although the correlations are low, with peak absolute values around 0.3, Fig. 4a does show a coherent La Niña pattern where the tropical eastern Pacific and central Indian Ocean are generally cooler, while warmer-than-normal SSTs prevail to the North of Australia and the South Pacific convergence zone. At the opposite phase, this first component is related to El Niño conditions.

The second slow DJF rainfall pattern and the associated circulation are shown in Fig. 3b. For this mode, we have chosen to show the global pattern of the covariance with the 500-hPa height field, because this better shows the connection between NZ rainfall variability and the anomalous circulation associated with the

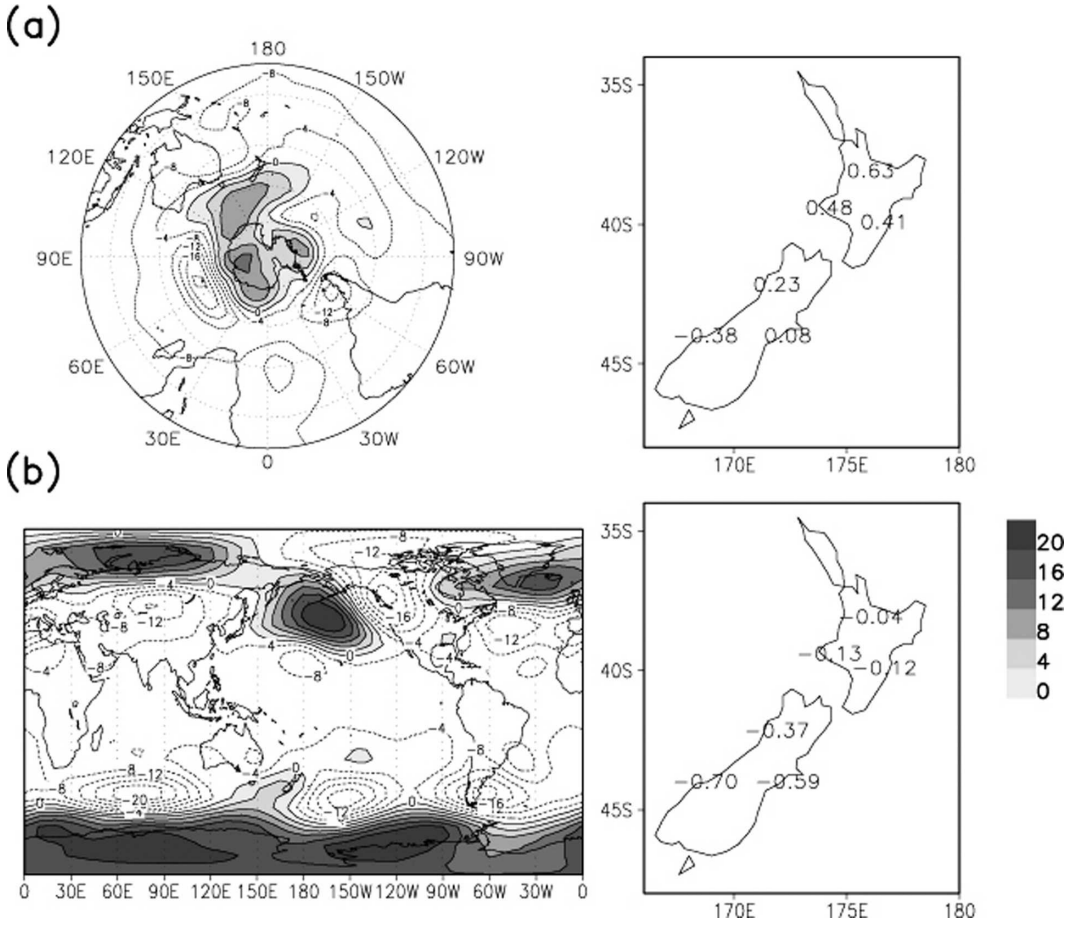

FIG. 3. As Fig. 1, but for DJF.

Australian monsoon. Locally, the 500-hPa height pattern has an anomalous high centered well south of New Zealand, with positive anomalies extending over much of the country. In response, NZ is drier everywhere, especially in the South Island. High pressure anomalies prevail throughout the southern polar regions, with lower pressure further equatorward with an obvious wavenumber-3 pattern, suggestive of the SAM [cf., e.g., with Fig. 8.3(a) of Kiladis and Mo 1998]. The one-point correlation map between SST and rainfall PC2 (Fig. 4b) shows little tropical SST forcing associated with this rainfall pattern.

As in Zheng and Frederiksen (2004), for their study of slow New Zealand DJF surface air temperature variability, the height field shows a distinctive Pacific–North American (PNA)-type teleconnection. Frederiksen and Frederiksen (1993a) found quasi-stationary global dynamical modes during DJF that coupled the Australian monsoon region to PNA extratropical variability. Outside of the Southern Hemisphere polar region, Fig. 3b is remarkably similar to these dynamical teleconnection patterns (see, e.g., Fig. 9a of Frederiksen and Frederiksen 1993a). This suggests some connection between this coupled pattern and Australian monsoon activity.

c. Intraseasonal patterns

The intraseasonal components of covariability are essentially unpredictable at the long range (a season or more ahead). As such they give an indication of the sources of uncertainty in seasonal predictions. The contribution of the intraseasonal components can be as large as the slow component, especially in the extratropics (Madden 1976; Zheng et al. 2000, 2004; Frederiksen and Zheng 2004). It is worthwhile reiterating that, in any study of coupled patterns using a standard SVD analysis of the seasonal mean data, the dominant coupled patterns will, in general, be combinations of our slow and intraseasonal components. Our methodology separates much of the intraseasonal contribution with the result that the slow components will, in general, reflect the more potentially predictable

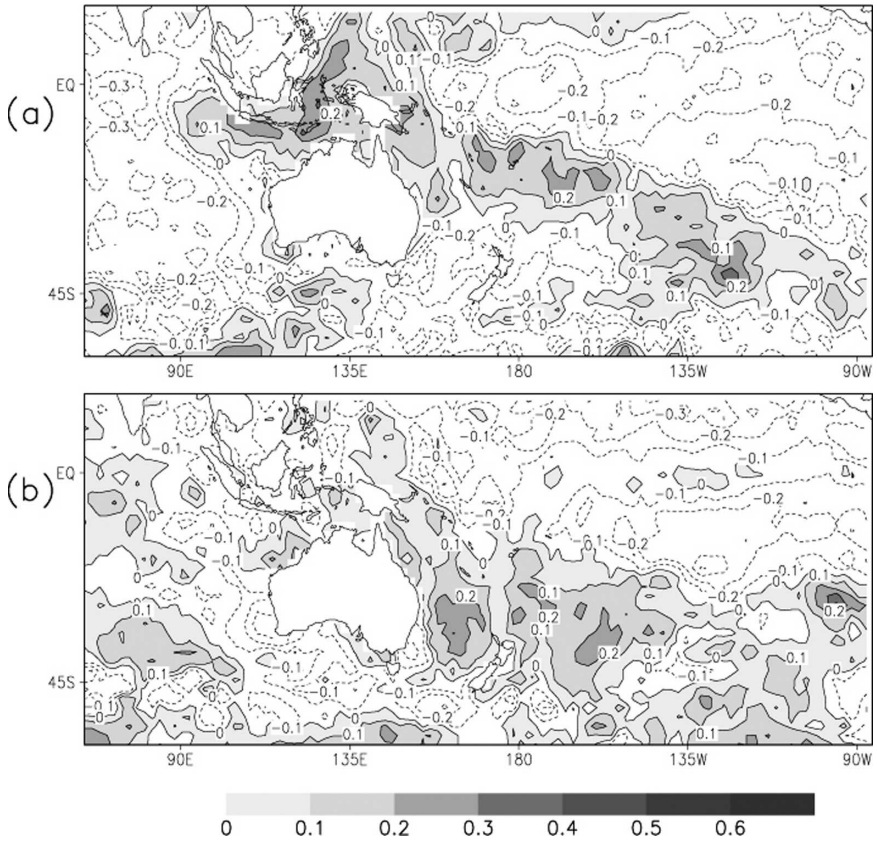

FIG. 4. As Fig. 2, but for DJF.

characteristics of the coupled variability. As such, they are the patterns that should be used as a guide in deriving any predictive scheme.

In JJA, the first two dominant coupled intraseasonal modes explain 60% (33% and 27%, respectively) of the covariability in the intraseasonal component in New Zealand rainfall and Southern Hemisphere MSLP. The first intraseasonal JJA rainfall pattern and the associated circulation are shown in Fig. 5a. The 500-hPa height shows a distinctive wavenumber-3 pattern and a very deep anomalous trough over the polar region, typically associated with SAM. Negative anomalies over southern New Zealand direct enhanced westerly/southwesterly winds throughout the country. As a consequence, New Zealand is generally wetter, especially along the west coast, west of the New Zealand Alps. In the opposite phase, drier conditions prevail over the country with higher-than-normal heights.

Figure 5b shows the second intraseasonal JJA rainfall pattern and the associated circulation. The height field has a distinct and localized meridional dipole structure west of New Zealand. Such a pattern is typical of blocking in the Tasman Sea region (see, e.g., Fig. 5a of Frederiksen and Frederiksen 1993b). At the phase shown, the anomalous trough–ridge pair directs anomalous easterlies/northeasterlies over New Zealand, resulting in enhanced rainfall on the east coast and depressed rainfall in the southwest, west of the New Zealand Alps. To confirm that this coupled pattern is associated with blocking, we have used the NCEP–NCAR reanalysis 500-hPa zonal wind data to derive a Southern Hemisphere blocking index based on that used by the Australian Bureau of Meteorology. This index is based on the zonal wind u at 500 hPa and is defined by $0.5[u(25°\text{S}) + u(30°\text{S}) + u(55°\text{S}) + u(60°\text{S}) - u(40°\text{S}) - u(50°\text{S}) - 2u(45°\text{S})]$. The PC associated with this 500-hPa height pattern has a correlation of 0.6 (at 157.5E) with this index.

In DJF, the first two dominant intraseasonal-coupled patterns explain 74% (41% and 33%, respectively) of the covariability in the intraseasonal component. The first intraseasonal rainfall pattern and the associated surface circulation are shown in Fig. 6a. The height field shows a distinctive wave train with a high center over New Zealand, associated with drier conditions everywhere. In the opposite phase, wetter conditions prevail. Such patterns are fairly common in the Southern Hemisphere and occur at both interannual and intraseasonal

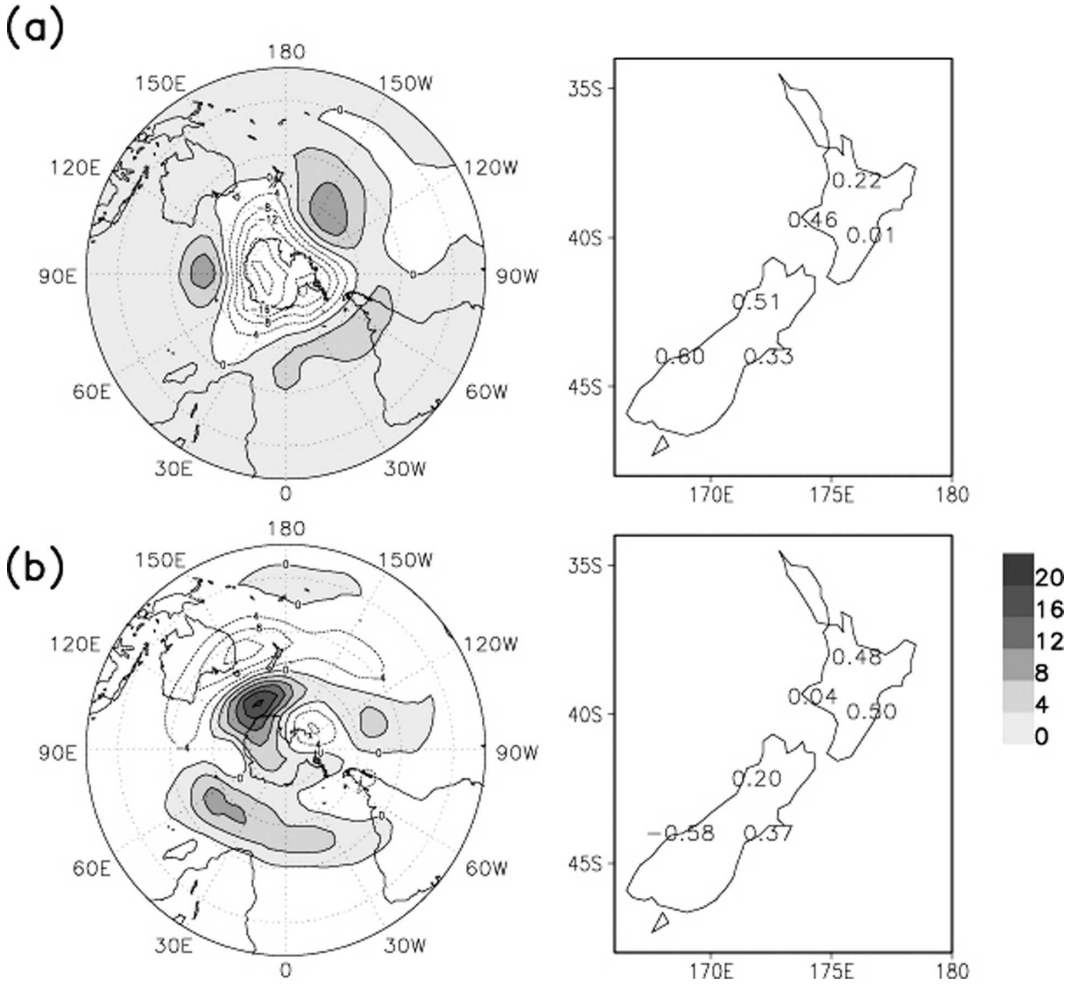

FIG. 5. Coupled EOF patterns for the intraseasonal modes: (a) JJA 500-hPa height and NZ rainfall EOF1, and (b) JJA 500-hPa height and NZ rainfall EOF2. Contour interval is 4 m and positive contours are shaded.

frequencies [see, e.g., the discussion in Kiladis and Mo 1998, and their Figs. 8.3(c) and 8.9(a), (b)].

The second intraseasonal DJF rainfall pattern and the associated circulation are shown in Fig. 6b. The 500-hPa height pattern has a more zonally symmetric structure with heavy weighting in the polar region and a wavenumber-4 pattern in the extratropics. In these respects it has many of the characteristics associated with the intraseasonal variability of SAM in summer. Frederiksen and Frederiksen (1993b), in their instability study of the Southern Hemisphere circulation, found a number of modes with similar horizontal structures, some of which were stationary and others of which had intraseasonal periods. This coupled mode appears to be related to intraseasonal variability associated with SAM. Negative height anomalies centered over the southwest of the South Island are responsible for the significantly wetter conditions in this region. Implied enhanced southwesterlies over the North Island are associated with drier conditions in the northnortheast. In the opposite phase, implied northeasterly wind anomalies over the North Island bring wetter conditions, while an anomalous ridge over the South Island is associated with drier conditions.

5. Prediction experiments

In section 3b, we showed that if the slow rainfall PC can be predicted, then the New Zealand seasonal rainfall anomaly field could be predicted by Eq. (12). As discussed above, the top two dominant slow rainfall/MSLP patterns in both JJA and DJF explain a substantial amount of the covariability of the slow components. In this study, we will try to predict the top two slow rainfall PCs using as predictors those circulation and SST relationships revealed in the analysis of the

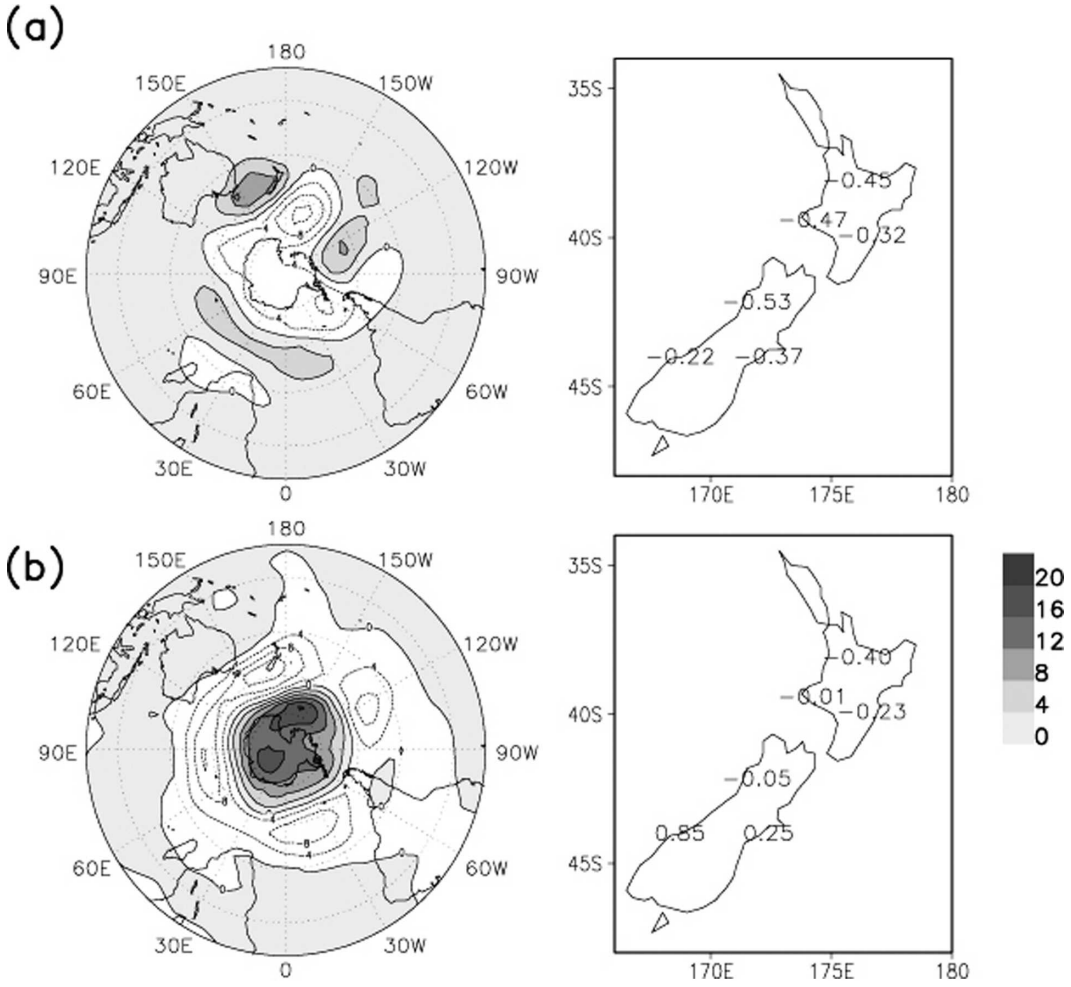

FIG. 6. As in Fig. 5 but for DJF.

coupled patterns, while we will set the other four PCs to be zero.

We choose 1953–92 as the training period and 1993–2000 as the verification period of our predictive scheme. The slow rainfall patterns for the training period are those estimated in sections 4a–4b. Because the rainfall is known in the training period the corresponding PCs are also known. The aim then is to estimate the PC time series in terms of a set of relevant predictors and to use this functional relationship to estimate the seasonal rainfall anomalies in the verification period. Here, we estimate the relationship between the PCs and the predictors using linear regression. To give a little more flexibility, we will consider both one-season-lead and one-month-lead values of our circulation and SST predictors. We then use stepwise regression to further select which of the predictors are most appropriate to train the regression coefficients. The results are listed in Table 1.

It is perhaps worthwhile noting here that from Figs. 2 and 4, local New Zealand SSTs, the average of the SST over the region (30°–46°S, 160°E–170°W), following Mullan (1998), often appear to be possible predictors. One-season-, or one-month, leading local SSTs may, of course, predict a persistence of a circulation feature or a local SST that might force New Zealand climate in the next season. If the correlation coefficient between the leading local SSTs and rainfall PC is around 0.25 (corresponding to 10% significance in the Pearson correla-

TABLE 1. Prediction formulas for slow rainfall PCs.

Predictand	Predictors
JJA PC1	−0.703 98 + 0.038 49 × May Niño-3 SST
JJA PC2	1.162 00 − 0.052 19 × MAM central Indian SST
DJF PC1	0.323 07–0.027 83 × SON Niño-3 SST − 0.055 57 × Nov NZ SST
DJF PC2	2.591 − 5.420 × SON SAMI

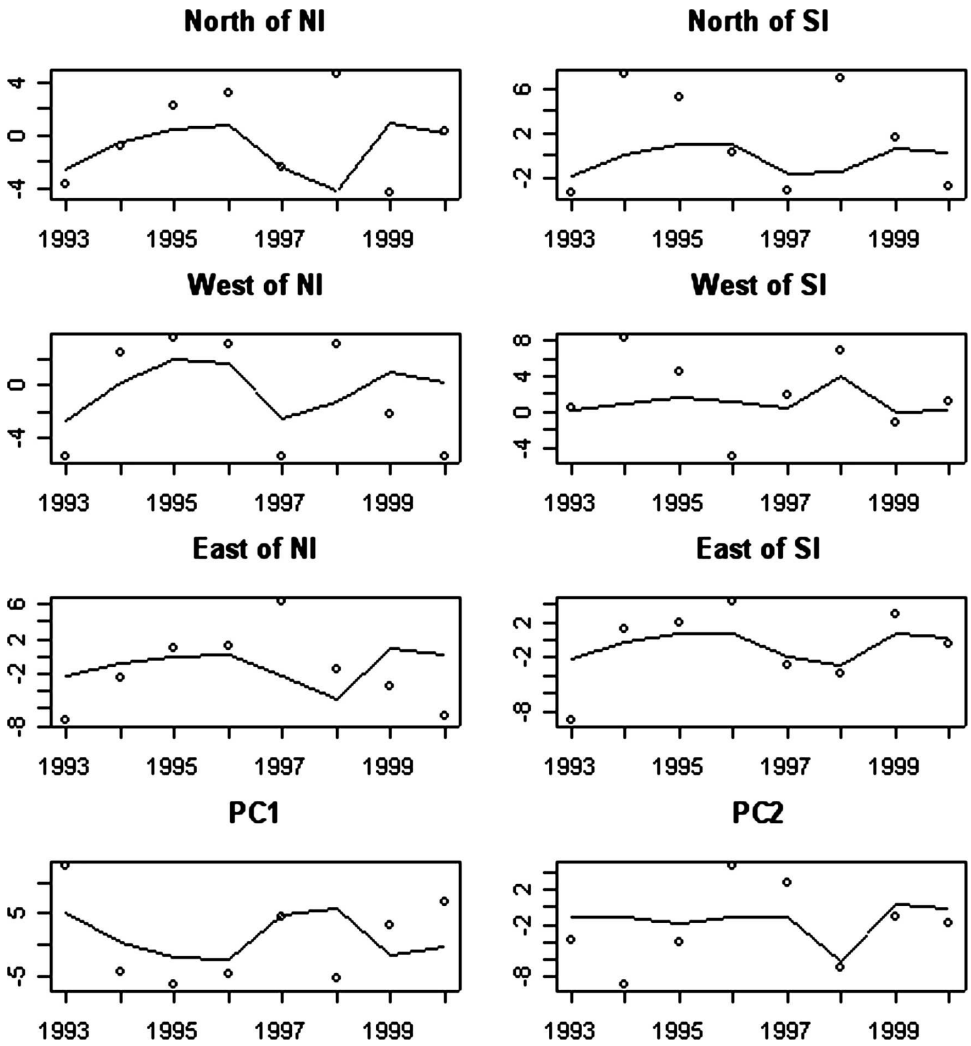

FIG. 7. Observations (dotted) and prediction (lined) time series of rainfall anomalies for each region and the slow rainfall PCs for JJA.

tion test) or more, then they could possibly be used as candidate predictors.

As we have shown in section 4a, the first JJA slow rainfall pattern is clearly associated with the interannual variability of ENSO and the local SSTs. Therefore, we considered the one-season-lead (MAM) and one-month-lead (May) Niño-3 (5°N–5°S, 90°–150°W) SSTs and NZ local SST as possible predictors of the PC. In this case, stepwise regression selected the May Niño-3 SST as being the best predictor rather than MAM. This is consistent with the fact that El Niño often changes phase in April, and therefore May Niño-3 SST is a better predictor of the phase of ENSO in JJA. Neither MAM nor May NZ local SST was selected as a predictor, presumably owing to the fact that they are significantly correlated with May Niño-3 SST. It is evident from the one-point correlation map (Fig. 2b) that central Indian Ocean SSTs, at leads of one month or a season, are possible predictors of the second JJA slow rainfall PC. We have defined a central Indian Ocean SST index that is the average of the SST over the region (0°–15°S, 60°–85°E), following Mullan (1998). In this case, the MAM index is the best predictor.

During DJF, ENSO variability and the leading NZ local SSTs are associated with the first DJF slow rainfall PC (see Fig. 4a). Therefore, the Niño-3 SSTs and New Zealand local SSTs, at one-month or one-season lead, are selected as possible predictors. The analysis shows that the SON Niño-3 index and November local New Zealand SSTs are the best predictors and both of them are significant at the 1% level.

The SAM is clearly related to the second DJF slow rainfall pattern (see section 4b), and therefore SAMI, at one-month or one-season lead, is a possible predic-

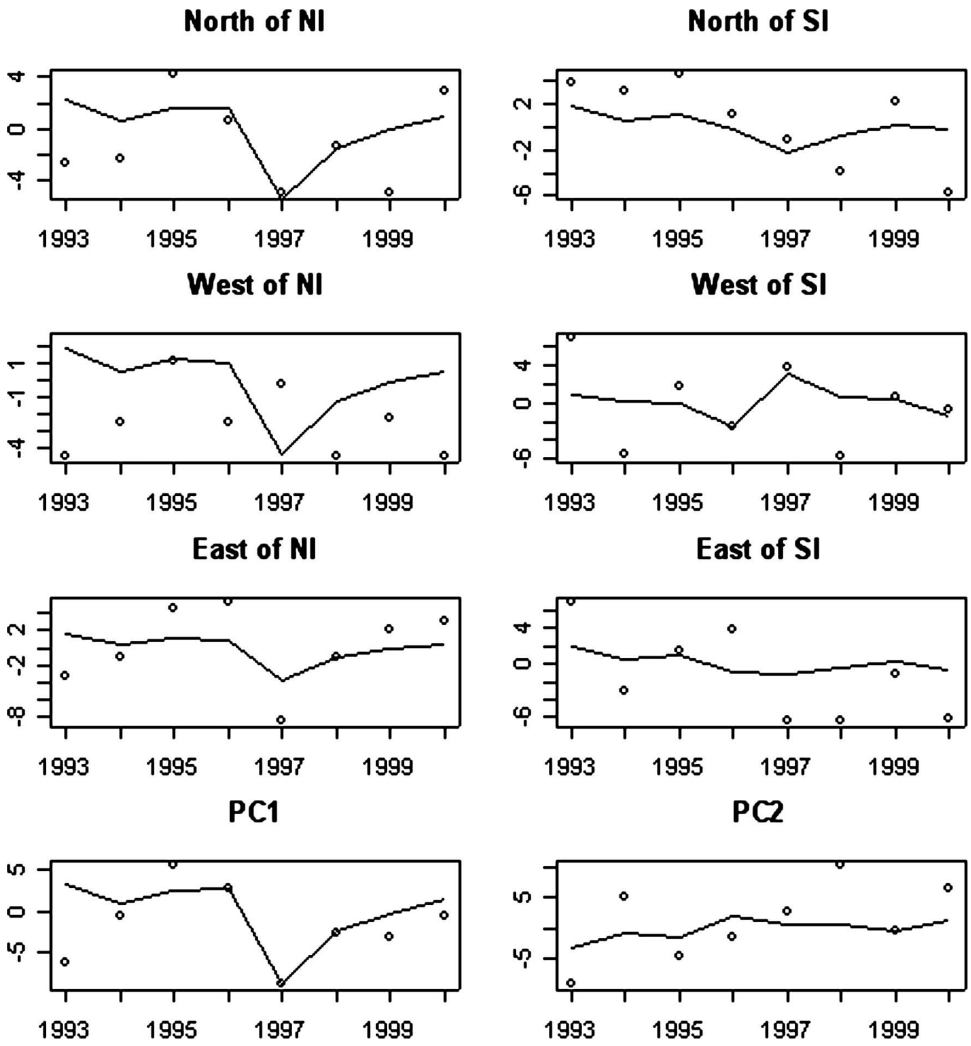

FIG. 8. As in Fig. 7, but for DJF.

tor. In this case, the analysis shows that the SON SAMI is the best predictor.

Generally speaking, to date the best prediction skill for NZ seasonal rainfall, in terms of the percentage explained variance [Eq. (14)], has been around 10% or less (Zheng and Renwick 2003). However, in this study, using the estimated PC relationships in Table 1, the percentage explained variance is 17% for NZ JJA rainfall and 20% for NZ DJF rainfall. The plots of observation against prediction are shown in Figs. 7–8.

We have also tried a commonly used alternative approach. Rather than predicting the slow rainfall PCs, we have tried an approach similar to that of Zheng and Renwick (2003), using stepwise regression to select the predictors for each of the six regional rainfalls individually. The same candidate predictors were used as for our analysis above. However, the percentage explained variance is −6% for JJA and 13% for DJF. Kidson and Gordon (1986) also studied the predictability of NZ rainfall PCs associated with surface circulations, and found no predictability during both JJA and DJF. In their case, the total rainfall and circulation fields were used in the analysis, whereas here we have implicitly based our predictive scheme on an understanding of the relationship between the slow components of these fields.

All of this suggests that forecasting the slow PCs is a better approach. We suspect that this is so, because the intraseasonal component of rainfall variability plays a role in reducing the predictability. In our method, this component is largely removed. Also, as a result, the slow PC is probably more likely to be closely related to large-scale coherent forcings and atmospheric teleconnections.

6. Conclusions

In this study, we have applied the methodology of Zheng and Frederiksen (2004) to identify important hemispheric circulation features that influence the predictable and unpredictable variability of JJA and DJF seasonal mean NZ rainfall. This has been done by using a decomposition of the cross-covariance matrix between NZ seasonal mean rainfall fields and the SH seasonal mean MSLP field into an intraseasonal and a slow component. Using this approach, we have gained a more quantitative understanding of the sources of predictability and uncertainty in NZ rainfall variability.

The analysis shows that the most important source of predictability in both austral summer and winter comes from the Southern Oscillation, with around 40% or more of the covariability in the rainfall and MSLP fields coming from this source. Two other important SH teleconnections—the wavenumber-3 pattern forced by Indian Ocean SST and the SAM—play a lesser role in austral winter and summer, respectively. One-point correlation maps between SSTs and the rainfall principal component time series of these coupled patterns have shown the importance of Niño-3, the central Indian Ocean, and local NZ SSTs in remotely, or locally, forcing much of this predictable variability.

The intraseasonal components of rainfall variability are related to well-known SH circulation features associated with intraseasonal internal dynamics. Thus, for example, in JJA, variability associated with the SH wavenumber-3 pattern associated with the intraseasonal variability of the SAM and blocking in the Tasman Sea region are most important. During DJF, variability associated with wave train disturbances and a wavenumber-4 pattern associated with the intraseasonal variability of the SAM are the two important SH circulations.

Based on this understanding, a statistical prediction scheme, using the slow rainfall PCs as predictands, has been proposed. Its initial application to seasonal prediction of NZ rainfall indicates that the scheme is promising, with a greater predictive skill than previously obtained. This is primarily so because in any study of coupled patterns using the total seasonal mean data, the dominant coupled patterns will, in general, be combinations of our slow and intraseasonal components. The methodology used here separates much of the intraseasonal contribution with the result that the slow components will, in general, reflect better the predictable characteristics of the coupled variability. Although nearly 20% of NZ rainfall variance is predicted by the proposed method, there is still 80% or more of the rainfall variance that cannot be predicted by this method. In future work, we plan to investigate the predictability of NZ rainfall and to test the skill of the proposed scheme using a cross-validation approach.

Acknowledgments. This work was supported by New Zealand Foundation for Research, Science and Technology (Contract C01X0202). We wish to thank BMRC for funding several visiting fellowships for XZ. We also wish to thank Drs. James Renwick and Brett Mullan, and two anonymous reviewers for useful comments, which have helped improve our presentation.

REFERENCES

Francis, R. I. C. C., and J. A. Renwick, 1998: A regression-based assessment of the predictability of New Zealand climate anomalies. *Theor. Appl. Climatol.,* **60,** 21–36.

Frederiksen, C. S., and X. Zheng, 2004: Variability of seasonal-mean fields arising from intraseasonal variability: Part II, Application to NH winter circulations. *Climate Dyn.,* **23,** 193–206.

Frederiksen, J. S., and C. S. Frederiksen, 1993a: Monsoon disturbances, intraseasonal oscillations, teleconnection patterns, blocking, and storm track of the global atmosphere during January 1979: Linear theory. *J. Atmos. Sci.,* **50,** 1349–1372.

——, and ——, 1993b: Southern Hemisphere storm tracks, blocking and low-frequency anomalies in a primitive equation model. *J. Atmos. Sci.,* **50,** 3148–3163.

Gordon, N. D., 1986: The Southern Oscillation and New Zealand weather. *Mon. Wea. Rev.,* **114,** 371–387.

Kalnay, E. M., and Coauthors, 1996: The NCEP/NCAR 40-Year Reanalysis Project. *Bull. Amer. Meteor. Soc.,* **77,** 437–471.

Karoly, D. J., 1989: Southern Hemisphere circulation features associated with El Niño-Southern Oscillation events. *J. Climate,* **2,** 1239–1252.

Kidson, J. W., and N. D. Gordon, 1986: Interannual variations in New Zealand temperature and precipitation patterns. *N. Z. J. Geophys.,* **29,** 363–375.

Kiladis, G. N., and K. C. Mo, 1998: Interannual and intraseasonal variability in the Southern Hemisphere. *Meteorology of the Southern Hemisphere*, *Meteor. Monogr.*, No. 49, Amer. Meteor. Soc., 307–336.

Madden, R. A., 1976: Estimates of the natural variability of time averaged sea level pressure. *Mon. Wea. Rev.,* **104,** 942–952.

——, 1981: A quantitative approach to long-range prediction. *J. Geophys. Res.,* **86,** 9817–9825.

Mullan, A. B., 1995: On the linearity and stability of Southern Oscillation-climate relationships for New Zealand. *Int. J. Climatol.,* **15,** 1365–1368.

——, 1998: Southern Hemisphere sea surface temperatures and their contemporary and lag association with New Zealand temperature and precipitation. *Int. J. Climatol.,* **18,** 817–840.

Rayner, N. A., D. E. Parker, E. B. Horton, C. K. Folland, L. V. Alexander, D. P. Rowell, E. C. Kent, and A. Kaplan, 2003: Globally complete analyses of sea surface temperature, sea ice, and night marine air temperature since the late nineteenth century. *J. Geophys. Res.,* **108,** 4007, doi:10.1029/2002JD002670.

Salinger, M. J., 1980: New Zealand climate: I. Precipitation patterns. *Mon. Wea. Rev.,* **108,** 1892–1904.

Thompson, D. W. J., and J. M. Wallace, 2000: Annular modes in the extratropical circulation. Part I: Month-to-month variability. *J. Climate,* **13,** 1000–1016.

Wilks, D. S., 1995: *Statistical Methods in the Atmospheric Sciences*. Academic Press, 467 pp.

Zheng, X., and C. S. Frederiksen, 1999: Validating interannual variability in an ensemble of AGCM simulations. *J. Climate,* **12,** 2386–2396.

——, and J. A. Renwick, 2003: A regression based scheme for seasonal forecasting of New Zealand temperature. *J. Climate,* **16,** 1843–1853.

——, and C. S. Frederiksen, 2004: Variability of seasonal-mean fields arising from intraseasonal variability: Part I, Methodology. *Climate Dyn.,* **23,** 177–191.

——, H. Nakamura, and J. A. Renwick, 2000: Potential predictability of seasonal means based on monthly time series of meteorological variables. *J. Climate,* **13,** 2591–2604.

——, M. Sugi, and C. S. Frederiksen, 2004: Interannual variability and predictability in an ensemble of climate simulations with the MRI-JMA AGCM. *J. Meteor. Soc. Japan,* **82,** 1–18.